processes

MDPI

Article

Molecular Dynamics Simulation of Phase Behavior of Fluid in Confined Nanopores

Jiahao Gao [1,2], Ke Zhang [1,2], Weifeng Lyu [1,2,*], Yu Zhang [1,2], Mingyuan Wang [1,2], Yaoze Cheng [1,2], Ao Li [3] and Xv Chen [1,2]

[1] Research Institute of Petroleum Exploration and Development, PetroChina Company Limited, Beijing 100083, China; gjiahao@petrochina.com.cn (J.G.)
[2] State Key Laboratory of Enhanced Oil Recovery, PetroChina Company Limited, Beijing 100083, China
[3] State Key Laboratory of Heavy Oil Processing, China University of Petroleum, Beijing 102249, China
* Correspondence: lweifeng@petrochina.com.cn

Abstract: The reservoir proportion with deep and low permeability, where oil and gas exist widely in nanopores, has been discovered increasingly in China. Affected by the nano-confinement effect, the phase behavior of fluid in nanopores varies with nanopore size rather than being constant. In this paper, the density, viscosity, and saturation pressure of pure and mixed fluids in nanopores are studied by molecular dynamics (MD) simulation combined with statistical physics. The feasibility of using the MD method to investigate fluid behavior in nanopores was verified with laboratory data. It was found that the fluids' phase behavior parameters in nanopores are lower than those in the bulk phase due to the confinement effect. The boundary of confinement effect (BCE) is defined as a size range of nanopores that separates the pore scale into the confinement scale and bulk scale. Each fluid has a specific BCE influenced by the molecular size of fluid. The phase behavior of crude oil in shale and tight oil reservoirs is most affected by the molecular adsorption and interaction energy between the fluid molecule and pore wall. Clarifying a specific BCE in shale reservoirs can significantly enhance the understanding of reservoirs and guide reservoir development strategies.

Keywords: phase behavior; nano-confinement effect; molecular dynamics; CCUS

check for updates

Academic Editor: Qingbang Meng

Received: 7 January 2025
Revised: 24 January 2025
Accepted: 5 February 2025
Published: 12 February 2025

Citation: Gao, J.; Zhang, K.; Lyu, W.; Zhang, Y.; Wang, M.; Cheng, Y.; Li, A.; Chen, X. Molecular Dynamics Simulation of Phase Behavior of Fluid in Confined Nanopores. *Processes* **2025**, *13*, 506. https://doi.org/10.3390/pr13020506

Copyright: © 2025 by the authors. Licensee MDPI, Basel, Switzerland. This article is an open access article distributed under the terms and conditions of the Creative Commons Attribution (CC BY) license (https://creativecommons.org/licenses/by/4.0/).

1. Introduction

Low-permeability, tight, and deep reservoirs account for more than half of the newly discovered oil and gas reserves in China in the recent period. Unconventional oil and gas resources represented by shale oil and gas have greatly changed the world energy supply pattern [1,2]. The shale revolution in North America has transformed the US from an oil and gas importer to an oil and gas exporter [3]. As China's oil and gas exploration and development industry continues to develop towards a high level, the object of oil and gas field development has also transitioned from the conventional oil and gas field to the unconventional oil and gas field [4]. Unconventional oil and gas generally have ultra-low permeability, high temperature, and high pressure. Therefore, oil and gas fluids exist in micropores and nanopores [5]. Affected by the confinement effect, the phase characteristics of oil and gas fluid in nanopores are obviously different from those in conventionally scaled pores [6,7]. The development of unconventional oil and gas is greatly limited by the lack of understanding of fluid phase characteristics in micropores and nanopores. Therefore, the study of oil and gas fluid phase characteristics affected by the confinement

effect in micropores and nanopores has an important guiding role for the development and utilization of unconventional oil and gas resources, like shale oil and gas.

In recent years, micro/nanofluidic technology and molecular dynamics simulation methods have been widely used to study the phase characteristics of fluid at the confinement scale. Micro/nanofluidic technology has the advantage of visualization and speed [8–10]. It studies the phase characteristics of oil and gas fluid in the flow channel by designing and machining the micro/nano flow channel on a chip. However, the conclusions of phase state studies conducted by different scholars under tens of nanometers using micro/nanofluidic technology are inconsistent and even conflicting. Parsa believed the hydrocarbon phase transition pressure is lower than the saturation pressure due to the significant limiting effect in a 50 nm channel [11]. However, Mehrdad argued that the confinement effect within a 50 nm channel is almost negligible [12]. Due to inconsistent standards of experimental devices, inaccurate pressure and temperature control, uncertain experiment sample quality, etc., the results of micro/nanofluidic experiments are often different. In addition, Ashish Mathur developed a procedure with nuclear magnetic resonance to measure the density of hydrocarbon gas in nanopores of shale reservoirs [13]. Guo's study observed the multiphase flow behaviors and phase change in CO_2 injection at pore-scale using microfluidics [14]. They suggested that effective huff-n-puff operations require a sufficient gas concentration to generate bubbles and an adequate pressure gradient to push the dissolved gas displacement. In Qian's study, the microscopic flow and displacement characteristics of CO_2 flooding and storage in heterogeneous formations were investigated using the microfluidic technique [15]. The interactions of the multiphase system include the dissolution and diffusion-mass transfer between CO_2 and crude oil and the dissolution between CO_2 and water, with the former being more intense than the latter. Obviously, although experimental techniques such as micro/nanofluidic technology have made breakthroughs in the field of microscopic phase characteristics research, there are still many shortcomings that need to be improved.

At the same time, molecular dynamics (MD) simulation methods have been used by many scholars to study and solve nanoscale problems that are difficult to apply to conventional experiments in oil and gas fields [16,17]. Welch and Mohammad found that alkanes were obviously blocked and sequestrated in channels with a diameter of 3 nm using molecular dynamics simulation [18]. Sashanka Sekhar Mandal investigated the phase behavior of associating fluids inside a heterogeneous slit pore with Monte Carlo simulation. In the case of an attractive pore surface, the narrower pore undergoes the vapor–liquid transition earlier than in the wider pore [19]. In Wang's study, molecular dynamics methods were used to simulate the process of CO_2 replacing shale oil in hydrated nanopores of inorganic, organic, and composite minerals. The CO_2-EOR mechanisms of dissolution, extraction, viscosity reduction, miscibility, and competitive adsorption were revealed [20]. The flow obstruction phenomenon still exists even under pressure of up to 350 bar. Obviously, molecular dynamics has the advantage of studying the microscopic hydrocarbon characteristics. Moreover, Song developed a three-phase flash algorithm considering the effect of nanopore confinement to study the mutual solubility and fluid properties [21]. It was found that when the confinement effect is considered, the density difference of the vapor-oleic phases decreases, and the interfacial tension of the vapor-oleic phases decreases.

However, there are still some limitations in the current investigations on the phase behavior of fluid in confined nanopores. (1) For pores smaller than 50 nm, physical experiments have not been able to form a uniform understanding of fluid phase behavior. (2) It is difficult to reveal the nano-confinement mechanism of fluids in physical experiments. (3) Most investigations only selected CO_2 for research instead of common formation fluid

components. Therefore, it is necessary to further study the mechanism and influencing factors of phase behavior of common fluids in confined nanopores.

In this paper, we investigated the density, viscosity, and saturation pressure (bubble point pressure) of four fluids inside nanopores affected by the nano-confinement effect, using the molecular dynamics method and statistical physics. The research results showed the change of phase behavior under eight different nanopore heights from 1 to 30 nm, obtained from 72 sets of simulations (10 simulations per set). A range of nanopore heights was proposed to determine the scale boundary between the bulk phase and confined phase. This paper analyzed the reason for confinement effects on fluid phase behavior at the molecular scale.

2. Models and Methodology

2.1. Model Establishment

We set up gas and oil located in different nanopore models imitating fluid under confined and non-confined spaces to investigate phase behavior variability. All the numerical models in this work, including the density model, viscosity model, and saturation pressure model, were built by the Material Studio (MS) software (version: Materials Studio 2020, Accelrys, San Diego, United States.). Given the dominant mineral composition of typical reservoirs, quartz was selected as the nanopore walls to reflect the real condition of the reservoirs as much as possible. The α-quartz was imported from MS and constructed as a quartz wall including 960 SiO_2 molecules with dimensions (XYZ) of 51 × 49 × 8.3 Å. Two quartz walls were hydroxylated on the surface and distributed parallel to the XY plane placed symmetrically into the nanopore model. At the initial moment, fluid molecules, with a certain number varying with the nanopore height, were placed in the slit of a nanopore. In all the nanopore models, periodic and reflective boundaries were applied in the x–y and z directions, respectively. For universality of formation and displacement fluids, we utilized CO_2, N_2, CH_4, and a mixture of C_{10} and CH_4 as representative fluid molecules packed into the slit of the nanopore to carry out research. During gas flooding, carbon dioxide, flue gas, and produced gas are often injected into the formation to improve the recovery efficiency of shale and low-permeability reservoirs. Therefore, in this paper, CO_2, N_2, and CH_4 molecules were selected to represent the above gases as the main research objects. Moreover, a mixture of C_{10} and CH_4 components was selected to represent light crude oil in shale and low-permeability reservoirs.

The prominent difference between the density, viscosity, and saturation pressure models is the state of the nanopore walls. In density models, the lower nanopore wall is fixed. However, a force F is applied to the upper wall in the -z direction, as shown in Equation (1).

$$F = P \cdot s \tag{1}$$

where P and s represent the fluid pressure after system stabilization and the area in the XY plane of the nanopore wall, equal to 45 bar and 25.04 nm^2, respectively. In viscosity models, the upper and lower nanopore walls are fixed simultaneously. According to the definition of saturation pressure, the saturation pressure is measured as the pressure at which the first bubble appears in the liquid, for mixtures that initially exist in liquid form. In saturation pressure models, the lower wall is fixed but the upper one wall is movable. A special point to note about saturation models is that the mixed fluid is in a miscible state initially and the upper wall moves upward slowly, resulting in an increase in volume of the nanopore and a reduction in pressure of the system. The state of the mixed fluid gradually changes from miscibility to saturation. The upper wall stops moving once the mixed fluid reaches phase equilibrium, when bubbles appear in the miscible fluid region. The diagrams of the viscosity, density, and saturation pressure models are shown in Figure 1.

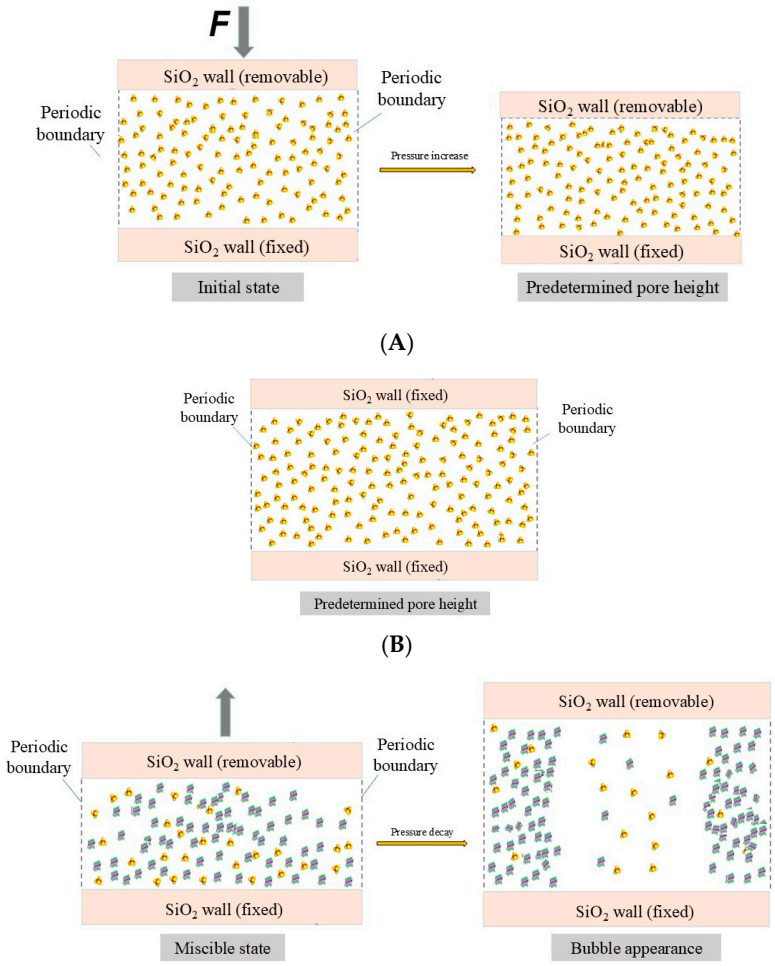

Figure 1. (**A**) Density, (**B**) viscosity and (**C**) saturation pressure models of fluid in a nanopore.

The Large-scale Atomic/Molecular Massively Parallel Simulator (LAMMPS, version: 28 Mar 2023, Sandia National Laboratories, Albuquerque, NM, USA) was utilized to perform all the MD simulations in this paper. The temperature and pressure of the system were selected from typical ultra-deep reservoirs (150 °C, 45 bar) to truly reflect the real oil and gas state and the thermodynamic state of displacement gas. The intermolecular non-bonded interactions, including short-range van der Waals (vdW) and long-range electrostatic interactions, are described by Equation (2). The simple resonance motive force is used to describe the intermolecular bond stretching and bond angle bending action, as shown in Equation (3). The PPPM method is used to solve the long range electrostatic force. The cut-off radius of the van der Waals force is 10 Å. The Lorentz–Berthelot mixing rule is used to calculate the Lennard–Jones potential energy between the crossed atoms in the system [22], as shown in Equation (4).

$$\phi(rij) = \begin{cases} 4\varepsilon_{ij}\left[\left(\frac{\sigma_{ij}}{rij}\right)^{12} - \left(\frac{\sigma_{ij}}{r_{ij}}\right)^{6}\right] + \frac{q_i q_j}{4\pi\varepsilon_0 r_{ij}} & (r_{ij} < r_{cut}) \\ 0 & (r_{ij} \geq r_{cut}) \end{cases} \quad (2)$$

$$\sigma_{ij} = \frac{(\sigma_{ii} + \sigma_{jj})}{2} \quad \varepsilon_{ij} = \sqrt{\varepsilon_{ii}\varepsilon_{jj}} \quad (3)$$

$$\begin{cases} E_b = k_b \cdot (r - r_0)^2 \\ E_\theta = k_\theta \cdot (\theta - \theta_0)^2 \end{cases} \quad (4)$$

In Equation (2), ε_{ij}, σ_{ij}, q_i, q_j, ε_0, r_{ij}, and r_{cut} represent the LJ well depth, zero-potential distance between atom I and j, charge of atom I, charge of atom j, dielectric constant of a vacuum, distance between the two atoms I and j, and truncation radius of the short range electrostatic force, respectively. In Equation (3), ε and σ are the energy and length parameters of the Lennard–Jones model. In Equation (4), k_b and k_θ represent the elongation and flexural elastic coefficients of the chemical bonds, respectively.

This investigation used different force field potential energy parameters to describe corresponding molecular groups. A flexible force field was used for CO_2 molecules [23], and the all-atom force field (OPLS-AA) was used for N_2 molecules. The ClayFF force field was used for SiO_2 molecules. The classical Optimized Potentials for Liquid Simulations (OPLS) force field was utilized for hydrocarbon molecules to expound dihedral angles, and the mathematical description of its potential energy is shown in Equation (5) [24]. A mixture composed of CH_4 and C_{10} (volume ratio = 1:4) was selected as the experimental fluid to represent crude oil as realistically as possible. In the simulations, the C_{10} molecule was modeled by the OPLS-UA (united-atom model) [25,26]. The united-atom model was utilized to greatly reduce the calculation amount and improve the calculation efficiency without affecting the accuracy of the results [27,28]. The simple harmonic vibration model was used to describe the interaction of bond angles. The potential energy parameters and charge values of each particle are shown in Table 1.

$$E(\varphi) = \frac{V_1}{2}[1 + \cos(\varphi)] + \frac{V_2}{2}[1 + \cos(2\varphi)] + \frac{V_3}{2}[1 + \cos(3\varphi)] \quad (5)$$

where V_1, V_2 and V_3 are the dihedral angle model coefficients and φ is the dihedral angle.

Table 1. Atomic potential energy parameters and charge values.

Molecule	Atom	ε	σ (Å)	q (e)	k_b	r_0 (Å)	k_θ	θ°
N_2	N	0.072	3.297	/	32.88	1.112	/	/
CO_2	C	0.056	3.03	0.6516	71.83	1.162	13.17	180
	O	0.16	2.8	−0.3258				
CH_4	C	0.066	3.5	−0.24	165.5	1.09	17.5	109.5
	H	0.03	2.5	0.06				
SiO_2	Si	0.04	4.05	0.6	/	/	/	/
	O	0.228	2.86	−0.3				
C_{10}	CH_3	0.176	3.91	/	261.5	1.53	63.42	112.4
	CH_2	0.119	3.91					

The units of ε, k_b, and k_θ are kcal/mol, kcal/(mol·Å^2), and kcal/(mol·rad^2), respectively.

To quantify the phase behavior of confined fluids in nanopores, we calculated the density, viscosity, and saturation pressure of fluids packed in nanopores with different heights. In density models, the fluid density is negatively related to the nanopore height h as shown in Equation (6), and the initial quantity of fluid molecules in the nanopore is constant.

$$\rho = \frac{M \cdot N}{N_A \cdot h \cdot s} \quad (6)$$

where M, N, N_A, h, and s are the molecular weight, number of molecules in the system, Avogadro's number, and nanopore height and area in the XY plane of the nanopore wall, respectively. For the hydrocarbon mixture composed of CH_4 and C_{10} (volume ratio = 1:4), an equivalent value of the mixture M_e is defined to describe the molecular weight, as shown in Equation (7).

$$M_e = 0.2M_{CH_4} + 0.8M_{C_{10}} \quad (7)$$

where M_{CH4} and M_{C10} represent the molecular weight of CH_4 and C_{10}, respectively.

In viscosity models, the fluid viscosity is calculated by the Green–Kubo formula based on the dynamic phase theory, as shown in Equation (8). It is found from Equation (8) that the fluid viscosity is positively related to the integral of the self-association function of the fluid shear stress tensor. Therefore, the fluid viscosity value can be obtained from the self-correlation integral.

$$\mu_{\alpha\beta} = \frac{1}{k_B T \cdot V} \int_0^\infty \left\langle J_{\alpha\beta}(t + t_0) \cdot J_{\alpha\beta}(t_0) \right\rangle \mathrm{d}t \tag{8}$$

where k_B, T, V, and $J_{\alpha\beta}$ stand for the Boltzmann constant, fluid temperature, fluid volume, and shear stress tensor of the fluid (shown in Equation (9)), respectively.

$$J_{\alpha\beta} = \sum_i^N m_i v_{ia} v_{i\beta} + \frac{1}{2} \sum_i^N \sum_{j \neq i}^N r_{ija} F_{ij\beta} \tag{9}$$

where m, v, r, and F are the atomic mass, atomic velocity, distance between atoms I and j, and interaction force, respectively.

In the saturation pressure model, the saturation pressure of the hydrocarbon mixture is obtained from the statistical mechanics as shown in Equation (10).

$$P = \frac{N \cdot k_B \cdot T}{V} + \frac{\sum_i^{N'} r_i \cdot f_i}{V} \tag{10}$$

where r_i, f_i, and V represent the coordinate vector, force vector, and fluid volume.

In all the simulations, the sampling interval of the self-correlation integral is 5 fs and the integral length is 10 ps. Each case under a specific nanopore height was obtained by an average of ten independent simulations to obtain stable and accurate test results. Each simulation begins with a particular initial condition, and the fluid molecules have a particular velocity field. The running curve of one case was obtained by averaging the running curves of ten simulations. Finally, the experimental value of the phase behavior was obtained by arithmetically averaging the average running curve values of the last 1 ns.

2.2. Model Validation

Due to the lack of laboratory data on fluid phase parameters under the nano-confinement effect, we built corresponding phase behavior models in the bulk phase and obtained values of the density, viscosity, and saturation pressure in the bulk phase compared with those from the NIST (National Institute of Standards and Technology) to identify the accuracy and feasibility of MD models. The validation results are shown in Table 2.

Table 2. Contrast of phase parameters between MD and NIST.

Fluid	Density (kg/m^3)			Viscosity (mPa·s)			Saturation Pressure (bar)		
	MD	NIST	RSD (%)	MD	NIST	RSD (%)	MD	NIST	RSD (%)
N_2	273.92	281.47	2.68	0.0328	0.0310	5.81	/	/	/
CO_2	678.86	650.69	4.33	0.0575	0.0542	6.09	/	/	/
CH_4	171.89	178.93	3.96	0.0253	0.0245	3.26	/	/	/
Mixture	681.03	625.00	8.20	0.2932	0.3320	13.23	46.07	50.58	9.80
Average RSD (%)			4.79			7.10			9.80

For density simulation, the periodic boundary is set in the Z direction instead of a quartz wall, as shown in Figure 2. The NPT ensemble is utilized during the simulation.

The density in the bulk phase from the results of the simulation and NIST are shown in Figure 3. The RSDs (Relative Standard Deviations) of experimental fluids between the MD and NIST range between 2.68% and 8.2%.

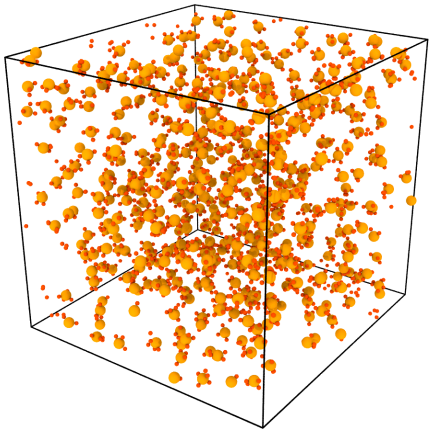

Figure 2. Experimental model of fluid density in the bulk phase.

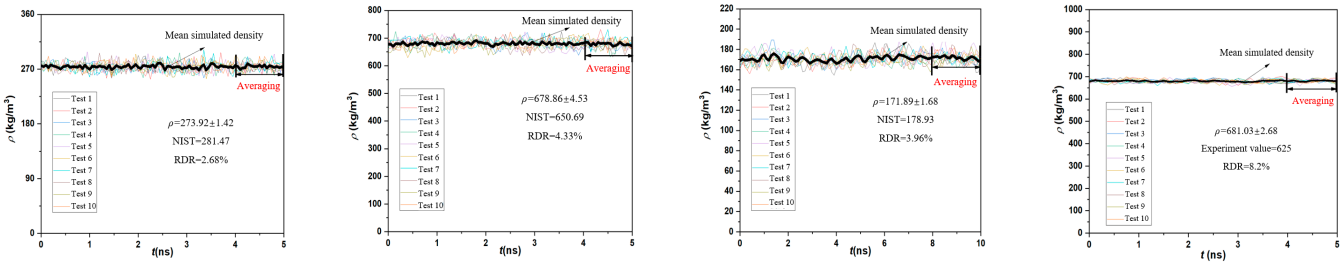

Figure 3. Density simulation experiments of (**A**) N_2, (**B**) CO_2, (**C**) CH_4, and (**D**) the fluid mixture.

For the viscosity model in the bulk phase, the only difference against the confined model is that the NVT ensemble is applied instead of the NPT ensemble. The contrast between the viscosity in the simulation and the NIST is shown in Figure 4, and the RSDs range from 3.26% to 13.23%.

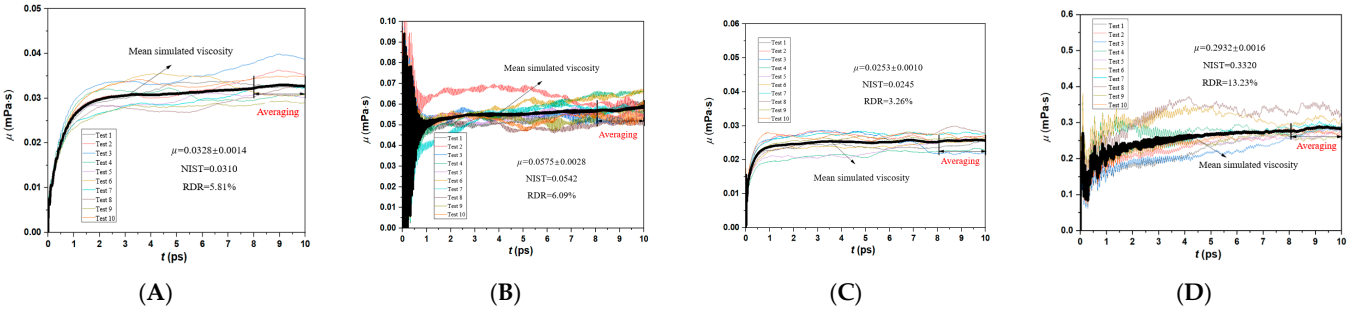

Figure 4. Viscosity simulation experiments of (**A**) N_2, (**B**) CO_2, (**C**) CH_4, and (**D**) the fluid mixture.

For the saturation pressure models in the bulk phase, the symmetrical quartz walls are removed and the periodic boundary is utilized in all directions compared to the nanopore models. The simulation process and results of saturation pressure in the bulk model are shown in Figure 5, and the RSD is 9.8%.

In conclusion, all results of the bulk phase models have RSDs less than 10% (density model = 4.84%, viscosity model = 7.10%, and saturation pressure = 9.80%) compared with the data from the NIST. Therefore, the reliability of the MD model to study the

phase behaviors of fluid can be verified, and we can conduct further research about phase behavior under nanopores.

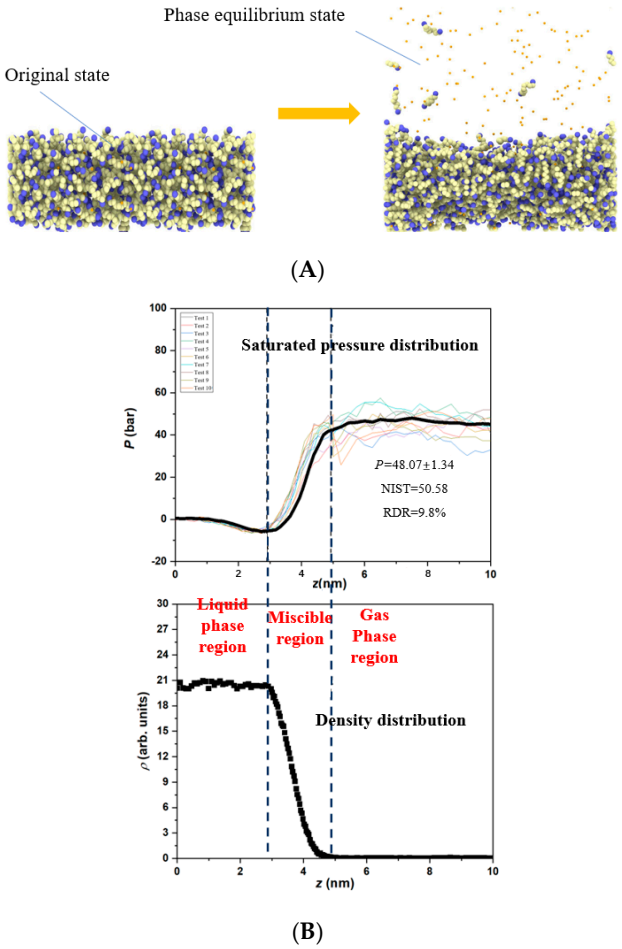

Figure 5. (**A**) Process and (**B**) results of the saturation pressure simulation experiment of the fluid mixture.

3. Results and Discussion

The phase behavior profiles of fluids (N_2, CO_2, CH_4, and the mixture) from bulk to confined nanopores at different heights are shown in Figure 6. All the kinds of behavior examined in this paper (density, viscosity, and saturation pressure) show deviations with the decrease of nanopore height. All the parameter values in nanopores are smaller than those in the bulk phase and show a trend of steady decrease at first, and then a rapid decrease, as shown in Figure 6 and Tables 3–5. When the pore height is 1–2 nm, the average density deviation from the bulk phase of four fluids is 24.32%. Among them, the deviations of CO_2 and N_2 have significant differences of 31.61% and 17.3%, which demonstrates that the sensitivity to nanopore height is discrepant, i.e., CO_2 > CH_4 > mixture > N_2, as shown in Figure 6A. Moreover, the viscosity of diverse fluid is more sensitive to the change of nanopore height, with an average deviation of 39.13%, namely mixture > CH_4 > CO_2 > N_2, as shown in Figure 6B. The saturation pressure of the mixture also has a decreasing trend from bulk to a nanopore of 1.78 nm, with a deviation of 25.44%. It is worth noting that the minimum pore height for N_2, CO_2, and CH_4 maintaining fluid in the bulk phase is about 20 nm, but the mixture's is about 30 nm. This demonstrates that the smaller nanopores have a significant confinement effect on fluid phase behavior. The values of the density, viscosity, and saturation pressure have a positive correlation with nanopore height.

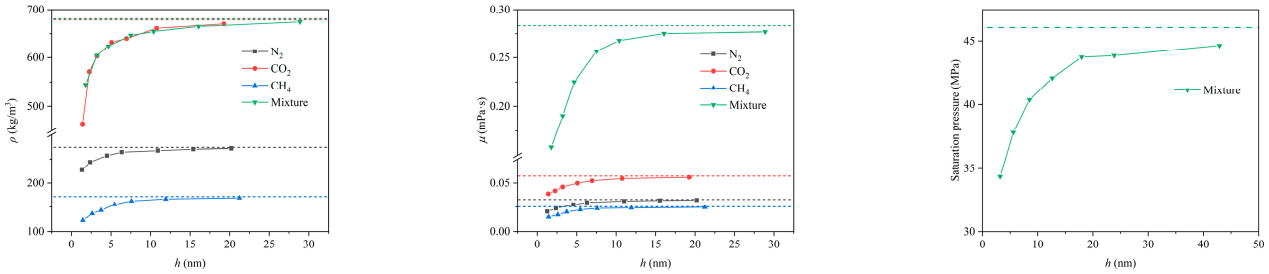

(**A**) (**B**) (**C**)

Figure 6. (**A**) Density, (**B**) viscosity, and (**C**) saturation pressure of fluids with different heights of nanopores. (The dashed lines represent the phase parameters under the volume phase).

Table 3. Density for nanopores with different heights.

EXP	N_2			CO_2			CH_4			Mixture		
	h	ρ	Dev.	h	ρ	Dev.	h	ρ	Dev.	h	ρ	Dev.
1	1.33	227.26	17.03	1.40	464.30	31.61	1.44	122.74	28.59	1.78	544.58	20.04
2	2.37	244.04	10.91	2.26	571.11	15.87	2.61	136.30	20.71	3.22	604.40	11.25
3	4.49	257.16	6.12	3.22	602.99	11.18	3.74	142.34	17.19	4.68	623.70	8.42
4	6.36	264.43	3.46	5.08	631.94	6.91	5.45	151.17	12.05	7.51	646.42	5.08
5	10.93	267.44	2.37	6.95	639.92	5.74	7.59	163.61	4.82	10.39	654.22	3.94
6	15.41	270.36	1.30	10.7	661.03	2.63	11.92	166.78	2.97	16.07	664.72	2.39
7	20.21	271.97	0.71	19.2	670.23	1.27	21.23	169.14	1.60	28.88	674.30	0.99
8	Bulk	273.92	0.00	Bulk	678.86	0.00	Bulk	171.89	0.00	Bulk	681.03	0.00

The units of *h*, ρ, and dev. are nm, kg/m^3, and %, respectively.

Table 4. Viscosity for nanopores with different heights.

EXP	N_2			CO_2			CH_4			Mixture		
	h	*μ*	Dev.	*h*	*μ*	Dev.	*h*	*μ*	Dev.	*h*	*μ*	Dev.
1	1.33	0.0203	38.11	1.40	0.0389	32.35	1.44	0.0147	41.90	1.78	0.1582	44.14
2	2.37	0.0225	31.40	2.26	0.0421	26.78	2.61	0.0170	32.81	3.22	0.1903	32.80
3	4.49	0.0292	10.98	3.22	0.0460	20.00	3.74	0.0199	21.34	4.68	0.2251	20.52
4	6.36	0.0307	6.40	5.08	0.0492	14.43	5.45	0.0222	12.25	7.51	0.2424	14.41
5	10.93	0.0308	6.10	6.95	0.0514	10.61	7.59	0.0235	7.11	10.39	0.2707	4.41
6	15.41	0.0311	5.18	10.7	0.0548	4.70	11.92	0.0241	4.74	16.07	0.2760	2.54
7	20.21	0.0311	5.18	19.2	0.0560	2.61	21.23	0.0247	2.37	28.88	0.2769	2.22
8	Bulk	0.0328	0.00	Bulk	0.0575	0.00	Bulk	0.0253	0.00	Bulk	0.2832	0.00

The units of *h*, *μ*, and dev. are nm, mPa·s, and %, respectively.

Table 5. Saturation pressure for nanopores with different heights.

EXP	Mixture		
	h	Saturation Pressure	Dev.
1	1.78	34.35	25.44
2	3.22	37.82	17.91
3	4.68	40.37	12.37
4	7.51	42.08	8.66
5	10.39	43.71	5.12
6	16.07	43.93	4.65
7	28.88	44.62	3.15
8	Bulk	46.07	0.00

The units of *h*, saturation pressure, and dev. are nm, bar, and %, respectively.

It is noted that there is a boundary, a certain range of nanopore heights, to split up the pore scale into two sections, the bulk phase and the nano-confined phase. We define the boundary of confinement effect (BCE) as a nanopore diameter range that separates the confinement scale and bulk scale. Figure 7 shows the change rate of fluid phase behavior with nanopore height, which suggests that the magnitude of change is gradually drastic with a decrease of nanopore height. The pink stripes in Figure 7A,B stand for a BCE between an h of 5 to 10 nm for pure fluids (N_2, CO_2, and CH_4), a transition zone of rate change. As h > BCE, fluid locates in the bulk area, showing phase behavior at the bulk scale. Oppositely, fluid in the confined area of h < BCE represents the phase behavior affected by the nano-confinement effect, with a rapid increase in the change rate. We notice that in the confined area, the change rate of density and viscosity is in the order of $CO_2 > N_2 > CH_4$, as shown in Figure 7A,B, opposite of the molecular diameter of $CO_2 < N_2 < CH_4$ (0.33 nm < 0.364 nm < 0.38 nm). Therefore, we point out that the change rate of phase behavior for a pure fluid is negatively correlated with the molecular diameter of the fluid.

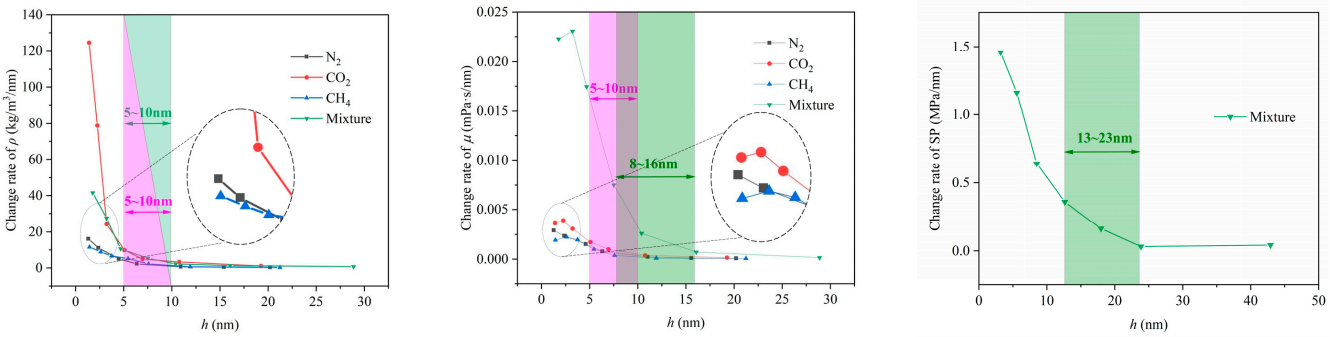

Figure 7. Change rate of (**A**) density, (**B**) viscosity, and (**C**) saturation pressure with different heights of nanopores. Pink stripe: BCE of pure fluid. Green Stripe: BCE of mixture. Oval frame: partial enlarged drawing of profiles for pure fluids.

As the green stripes in Figure 7 indicate, different profiles of mixture have nonequal ranges of transition zones, in obvious contrast with the equal BCE for pure components. Considering that changes of saturation pressure first occur in the range of 13–23 nm, we determine the value of the BCE of the mixture as 13–23 nm. The change rates of the mixture in viscosity and saturation pressure are much greater than those of pure fluids, due to the reason that the C_{10} diameter of 1.32 nm is considerably larger than those of pure molecules, which are within the range of 0.3 nm. Our research suggested that the BCEs of N_2, CO_2, and CH_4 are about 5–10 nm and the BCE of the mixture composed of CH_4 and C_{10} is about 13–23 nm, varied with the molecular diameter. These results correspond to Xu's study, which showed that n-butane's critical pore sizes, or BCE, range from 16 nm to 22 nm [29]. The critical temperature and pressure of n-butane decreases accompanied by sizes less than 16–22 nm. It can be found that the value of the BCE increases gradually with the increase of molecular size. This expands on previous knowledge that the phase behavior of confined fluids approached bulk behavior as the pore size increased to 10 nm [30]. At the confinement scale, the decrease in saturation pressure is beneficial for maintaining single phase crude oil, which theoretically facilitates the flow of oil.

It is worth noting that the density change rate of CO_2 in the confined area rises sharply, even more than the mixture, in Figure 7A. This can probably be attributed to the formation of CO_2 adsorption layers inside tiny nanopores near the quartz wall, enhancing the nano-confinement effect, because of the stronger interaction energy between the fluid and quartz molecules.

According to the above investigation, the phase behaviors of fluids in nanopores are obviously different from those in the bulk phase, affected by the nano-confinement effect. In molecular terms, the effect of the adsorption and interaction energy of the fluid-wall on phase behavior becomes more significant and plays a dominant role as the pore size decreases to a tiny nanopore. Fluid molecules in a nanopore can be divided into two parts, namely, the central molecules and the adsorbed molecules near the wall. In the bulk pores, the interaction energy among central molecules plays the main role in the whole system. The interaction energy between adsorbed molecules and wall molecules can be negligible due to the relatively small proportion of quantities. But as the pore size decreases to the nanometer scale, the number of fluid molecules mainly present in non-adsorption states is greatly reduced. The relative quantity ratio of adsorbed molecules increases rapidly and plays a dominant role in adsorption and energy distribution. Some scholars pointed out that a 0.38 nm monolayer adsorption of CH_4 forms in a slit-like nanopore [30]. The layer has a 1.8–2.5 times larger density than bulk methane. Therefore, the central molecules utilized to calculate density decline, contributing to a decrease in overall density. It is shown that the confinement effect enhances rapidly in the nanopores with heights smaller than the BCE. The changes in fluid phase behavior are essentially the result of changes in the distribution of molecules and energy within the nanopores. This study investigates the size boundary for common formation fluids between confined pores and bulk-phase pores in shale reservoirs from a new perspective, which help the reservoir develop specific EOR methods for different pore sizes and fluid characteristics.

4. Conclusions

In this study, MD simulations are performed to investigate the density, viscosity, and saturation pressure of common fluids affected by the confinement effect in nanopores. We compared the characteristics of phase behavior under the nano-confined and bulk phases to determine the BCE (boundary of confinement effect) of pore size. The main conclusions are as follows:

The phase behaviors, including the density, viscosity and saturation pressure, of N_2, CO_2, CH_4, and a mixture (CH_4:C_{10} = 1:4) are positively correlated with the height of nanopores in the size range of 1–30 nm. The specific trend of change is that, as the nanopores decrease in size, all the phase behavior first slowly decreases, and then rapidly decreases with the enhancement of the confinement effect. The confinement effect of nanopores on the fluid inside rapidly increases as the nanopore size decreases.

The phase behavior of a fluid shows different values from that under the bulk phase only as the fluid is located within nanopores smaller than the corresponding BCE. Each fluid has a specific BCE, which is influenced by the molecular size, the state of the adsorption layer, and the interaction energy between gas–wall molecules. The BCEs of carbon dioxide, nitrogen, and methane are about 5–10 nm, mainly due to their similar molecular diameters, ranging from 0.3–0.4 nm. The diameter of C_{10} in most molecules of the mixture is 1.32 nm, with a BCE of 13–23 nm, which is much larger than the former molecules.

Molecular adsorption and interaction energy have a more significant impact on the phase behavior and flow of crude oil in shale and tight oil reservoirs. Although in theory, the decrease in density, viscosity, and saturation pressure due to the significant confinement effect in nanopores is beneficial for the flow of crude oil, the development of tight and shale oil reservoirs is not fast in China. In the future, MD is needed to strengthen in-depth research on adsorption and energy perspectives.

Author Contributions: Data curation, Y.Z.; Software, M.W.; Writing—review & editing, A.L.; Investigation, Y.C.; Resources, W.L.; Supervision, K.Z.; Project administration, X.C.; Writing—original draft, J.G. All authors have read and agreed to the published version of the manuscript.

Funding: This research was funded by Science and Technology Research Project of PetroChina Company Limited, Research on enhanced oil recovery technology by multi-component gas flooding (2023ZZ0410) and the Major national science and technology projects, Research on comprehensive regulation technology of CO_2 miscible enhanced oil recovery (2024ZD1406601).

Data Availability Statement: The original contributions presented in this study are included in the article. Further inquiries can be directed to the corresponding author.

Conflicts of Interest: Authors Jiahao Gao, Ke Zhang, Weifeng Lyu, Yu Zhang, Mingyuan Wang, Yaoze Cheng and Xv Chen were employed by the PetroChina Co., Ltd. The remaining authors declare that the research was conducted in the absence of any commercial or financial relationships that could be construed as a potential conflict of interest. The PetroChina Co., Ltd., had no role in the design of the study; in the collection, analyses, or interpretation of data; in the writing of the manuscript, or in the decision to publish the results.

Abbreviations

The following abbreviations are used in this manuscript.

MD	Molecular Dynamics
BCE	Boundary of confinement effect
RSD	Relative Standard Deviation

References

1. Jia, C.; Zheng, M.; Zhang, Y. Unconventional hydrocarbon resources in China and the prospect of exploration and development. *Pet. Explor. Dev.* **2012**, *39*, 139–146. [CrossRef]
2. Sun, L.; Zou, C.; Jia, A.; Wei, Y.; Zhu, R.; Wu, S.; Guo, Z. Development characteristics and orientation of tight oil and gas in China. *Pet. Explor. Dev.* **2019**, *46*, 1015–1026. [CrossRef]
3. Le, M. An assessment of the potential for the development of the shale gas industry in countries outside of North America. *Heliyon* **2018**, *4*, e00516. [CrossRef] [PubMed]
4. Sun, C.; Nie, H.; Dang, W.; Chen, Q.; Zhang, G.; Li, W.; Lu, Z. Shale Gas Exploration and Development in China: Current Status, Geological Challenges, and Future Directions. *Energy Fuels* **2021**, *35*, 6359–6379. [CrossRef]
5. Nie, H.; Chen, Q.; Zhang, G.; Sun, C.; Wang, P.; Lu, Z. An overview of the characteristic of typical Wufeng–Longmaxi shale gas fields in the Sichuan Basin, China. *Nat. Gas Ind. B* **2021**, *8*, 217–230. [CrossRef]
6. Du, F.; Bahareh, N. Estimating Diffusion Coefficients of Shale Oil, Gas, and Condensate with Nano-Confinement Effect. In Proceedings of the SPE Eastern Regional Meeting, Charleston, WV, USA, 15–17 October 2019. [CrossRef]
7. Wu, S.; Li, Z.; Wang, Z.; Sarma, H.K.; Zhang, C.; Wu, M. Investigation of CO_2/N_2 injection in tight oil reservoirs with confinement effect. *Energy Sci. Eng.* **2020**, *8*, 1194–1208. [CrossRef]
8. Bao, B.; Riordon, J.; Mostowfi, F.; Sinton, D. Microfluidic and nanofluidic phase behaviour characterization for industrial CO_2, oil and gas. *Lab Chip* **2017**, *17*, 2740–2759. [CrossRef]
9. Zhang, Y.; Zhou, C.; Qu, C.; Wei, M.; He, X.; Bai, B. Fabrication and verification of a glass-silicon-glass micro-/nanofluidic model for investigating multi-phase flow in shale-like unconventional dual-porosity tight porous media. *Lab Chip* **2019**, *19*, 4071–4082. [CrossRef]
10. Liu, S.; Ma, Y.; Bai, B. Flow patterns of oil–water two-phase flow during pressure-driven process in nanoscale fluidic chips. *Microfluid. Nanofluidics* **2018**, *22*, 39. [CrossRef]
11. Parsa, E.; Yin, X.; Ozkan, E. Direct Observation of the Impact of Nanopore Confinement on Petroleum Gas Condensation. In Proceedings of the SPE Annual Technical Conference and Exhibition, Society of Petroleum Engineers, Houston, TX, USA, 27–30 September 2015. [CrossRef]
12. Mehrdad, A.; Hadi, N.; Debjyoti, B. Experimental investigation of confinement effect on phase behavior of hexane, heptane and octane using lab-on-a-chip technology. *Fluid Phase Equilibria* **2016**, *423*, 25–33. [CrossRef]
13. Mathur, A.; Ali, S.; Ali, M.; Belanger Chad Vivek, R. *Hydrocarbon Gas Behavior in Nano Pore Confinement Organic Shale Systems*; SPWLA: Houston, TX, USA, 2020. [CrossRef]
14. Guo, Y.; Liu, F.; Qiu, J.; Xu, Z.; Bao, B. Microscopic transport and phase behaviors of CO_2 injection in heterogeneous formations using microfluidics. *Energy* **2022**, *256*, 124524. [CrossRef]

15. Qian, C.; Rui, Z.; Liu, Y.; Zhou, K.; Du, K.; Zhao, Y.; Zou, J.; Song, K.; Li, X. Microfluidic investigation on microscopic flow and displacement behavior of CO_2 multiphase system for CCUS-EOR in heterogeneous porous media. *Chem. Eng. J.* **2025**, *505*, 159135. [CrossRef]
16. Bikai, J.; Ran, B.; Hadi, N. Molecular simulation of the pore size distribution effect on phase behavior of methane confined in nanopores. *Fluid Phase Equilibria* **2017**, *452*, 94–102. [CrossRef]
17. Mohamed, M.; Mashhad, F.; Huang, L. System Density of Oil-Gas Mixtures: Insights from Molecular Simulations. In Proceedings of the SPE Annual Technical Conference and Exhibition, San Antonio, TX, USA, 9–11 October 2017. [CrossRef]
18. Welch, W.R.; Piri, M. Molecular Dynamics Simulations of Retrograde Condensation in Nanoporous Shale. In Proceedings of the SPE/AAPG/SEG Unconventional Resources Technology Conference, San Antonio, TX, USA, 20–22 July 2015. [CrossRef]
19. Sashanka, S.M.; Sudhir, K.S.; Sandip, K. Effect of nanopore network connectivity on the phase behavior of confined associating fluids. *Fluid Phase Equilibria* **2025**, *588*, 114235. [CrossRef]
20. Wang, L.; Zhang, Y.; Zou, R.; Zou, R.; Yuan, Y.; Huang, L.; Liu, Y.; Meng, Z. Dynamics of oil–CO_2–water three-phase under the nanopore confinement effect: Implications for CO_2 enhanced shale oil recovery and carbon storage. *Sep. Purif. Technol.* **2025**, *354*, 128892. [CrossRef]
21. Song, Y.; Gu, S.; Song, Z.; Zhang, Z.; Chang, X.; Guo, J. Effect of confinement on the three-phase equilibrium of water-oil-CO_2 mixtures in nanopores. *Pet. Sci.* **2022**, *19*, 203–210. [CrossRef]
22. Daan, F.; Berend, S. *Understanding Molecular Simulation: From Algorithms to Applications*; Academic Press: Cambridge, MA, USA, 1996.
23. Cygan, R.T.; Romanov, V.N.; Myshakin, E.M. Molecular Simulation of Carbon Dioxide Capture by Montmorillonite Using an Accurate and Flexible Force Field. *J. Phys. Chem. C* **2012**, *116*, 13079–13091. [CrossRef]
24. Jorgensen, W.L.; Maxwell, D.S.; Tirado-Rives, J. Development and Testing of the OPLS All-Atom Force Field on Conformational Energetics and Properties of Organic Liquids. *J. Am. Chem. Soc.* **1996**, *118*, 11225–11236. [CrossRef]
25. Vekeman, J.; Faginas-Lago, N.; Lombardi, A.; Sánchez de Merás, A.; García Cuesta, I.; Rosi, M. Molecular Dynamics of CH_4/N_2 Mixtures on a Flexible Graphene Layer: Adsorption and Selectivity Case Study. *Front. Chem.* **2019**, *7*, 386. [CrossRef]
26. William, L.; Jeffry, D.; Carol, J. Optimized intermolecular potential functions for liquid hydrocarbons. *J. Am. Chem. Soc.* **1984**, *106*, 6638–6646. [CrossRef]
27. Peng, F.; Wang, R.; Guo, Z.; Feng, G. Molecular dynamics simulation to estimate minimum miscibility pressure for oil with pure and impure CO_2. *J. Phys. Commun.* **2018**, *2*, 115028. [CrossRef]
28. Mutailipu, M.; Liu, Y.; Jiang, L.; Zhang, Y. Measurement and estimation of CO_2–brine interfacial tension and rock wettability under CO_2 sub-and super-critical conditions. *J. Colloid Interface Sci.* **2019**, *534*, 605–617. [CrossRef]
29. Xu, Z.; Huang, L.; Yang, Q.; Feng, X.; Tian, B.; Chen, Q.; Qiu, X.; Wang, L.; Liu, Y.; Ning, Z.; et al. Coupling effect of fluid molecular structure and nanoporous structure on the confined phase behavior of butane isomers in shale nanopores. *Fuel* **2025**, *379*, 132983. [CrossRef]
30. Ambrose, R.J.; Hartman, R.C.; Diaz-Campos, M.; Akkutlu, I.Y.; Sondergeld, C.H. Shale Gas-in-Place Calculations Part I: New Pore-Scale Considerations. *SPE J.* **2012**, *17*, 219–229. [CrossRef]

Disclaimer/Publisher's Note: The statements, opinions and data contained in all publications are solely those of the individual author(s) and contributor(s) and not of MDPI and/or the editor(s). MDPI and/or the editor(s) disclaim responsibility for any injury to people or property resulting from any ideas, methods, instructions or products referred to in the content.